1995

Zero-Temperature Dynamics of the One-Dimensional *XXZ* and *t-J* Models: A Weak-Coupling Continued-Fraction Analysis

V. S. Viswanath
University of Rhode Island

Shu Zhang
University of Rhode Island

See next page for additional authors

Citation/Publisher Attribution
Viswanath, V. S., Zhang, S., Müller, G., & Stolze, J. (1995). Zero-temperature dynamics of the one-dimensional XXZ and t-J models: a weak-coupling continued-fraction analysis. *Phys. Rev. B*, 51(1), 368-380. doi: 10.1103/PhysRevB.51.368
Available at: http://dx.doi.org/10.1103/PhysRevB.51.368

Zero-temperature dynamics of the one-dimensional XXZ and t-J models: A weak-coupling continued-fraction analysis

V.S. Viswanath,* Shu Zhang, and Gerhard Müller
Department of Physics, The University of Rhode Island, Kingston, Rhode Island 02881-0817

Joachim Stolze
Physikalisches Institut, Universität Bayreuth, 95440 Bayreuth, Germany
(Received 22 June 1994; revised manuscript received 15 August 1994)

We use the recursion method to study the spectral and dynamical properties of the one-dimensional (1D) $s = 1/2$ XXZ model with planar anisotropy at $T = 0$. Distinct methods of continued-fraction analysis have been developed for the weak-coupling and strong-coupling regimes of the corresponding lattice fermion system. The weak-coupling analysis presented here yields detailed information on the spectral-weight distribution in dynamic structure factors and spin autocorrelation functions, notably on the infrared singularities produced by critical fluctuations, and on the bound states for the case of attractive fermion interaction. The same method is then applied to the charge dynamics of the 1D t-J model for strongly correlated electrons. There it yields similar yet distinct results in the regime of weak exchange coupling. The results for renormalized bandwidths of particle-hole excitations are consistent with available results for charge velocities, and the results for the infrared exponent in the charge dynamic structure factor agree with existing results for the exponent of the equal-time charge correlation function.

I. INTRODUCTION

Studies of cooperative phenomena in quantum many-body systems of interacting degrees of freedom are often classified into *weak-coupling* and *strong-coupling* approaches according to criteria that vary somewhat from method to method. The main goal of our investigation is to demonstrate that the recursion method can be successfully employed for the study of nontrivial problems in quantum many-body dynamics in both the weak-coupling and strong-coupling regimes of the underlying model system. In a companion paper,[1] we have already demonstrated the usefulness of the recursion method coupled with a *strong-coupling continued-fraction analysis* in an application to the $T = 0$ dynamics of the one-dimensional (1D) and 2D $s = 1/2$ XXZ antiferromagnets. Here we use the same method, but now combined with a *weak-coupling continued-fraction analysis*, for a comparative study of the dynamical properties in the ground state of two models with physically interesting weak-coupling regimes: the 1D $s = 1/2$ XXZ and t-J models.

The XXZ model for a magnetic insulator with uniaxially anisotropic exchange coupling between nearest-neighbor spins,

$$H_{XXZ} = \sum_{l=1}^{N} \{J_\perp (S_l^x S_{l+1}^x + S_l^y S_{l+1}^y) + J_z S_l^z S_{l+1}^z\}, \quad (1.1)$$

can be mapped via the Jordan-Wigner transformation onto a system of interacting lattice fermions (sometimes called the t-V model).[2] The XX model ($J_z/J_\perp = 0$) corresponds to the case of free fermions. The parameter $J_z/J_\perp$, which controls the anisotropy in spin space, is the coupling constant in the fermion representation.

The dynamic structure factor

$$S_{zz}(q,\omega) = N^{-1} \sum_{l,n} e^{-iqn} \int_{-\infty}^{+\infty} dt\, e^{i\omega t} \langle S_l^z(t) S_{l+n}^z \rangle \quad (1.2)$$

is related to a two-particle Green's function for the lattice fermions.[3,4] In the noninteracting case ($J_z/J_\perp = 0$), the particle-hole excitations of free lattice fermions are the only ones that contribute to $S_{zz}(q,\omega)$ at $T = 0$. They form a frequency band of finite width.

In a typical weak-coupling approach, the fermion coupling is taken into account more or less summarily. The dynamically relevant excitation spectrum of $S_{zz}(q,\omega)$ remains confined to a finite band. The effects of interaction at this level include renormalized two-particle excitation energies, modified line shapes and band-edge singularities, and the formation of bound states.

In a strong-coupling approach, by contrast, the dynamically relevant excitations in $S_{zz}(q,\omega)$ are truly collective in nature. In general, they involve arbitrarily many fermions and thus are spread over a frequency band of infinite width. A meaningful description of phase changes must involve these collective modes. This succinct characterization of the two regimes is borne out not only in the framework of the recursion method but also in the context of other methods that have been used for the study of the $T = 0$ dynamics of H_{XXZ}.

The t-J model for strongly correlated electrons has gained prominence chiefly in the context of oxide high-T_c superconductivity as a 2D application. It was designed

as an approximation to the Hubbard model for the case of very strong on-site repulsion—a model which strictly prohibits double occupancy of electrons on any site of the lattice.[5,6] The t-J Hamiltonian for a 1D lattice can be expressed in the form

$$H_{t\text{-}J} = -t \sum_{\sigma=\uparrow,\downarrow} \sum_{l=1}^{N} \left\{ \tilde{c}^{\dagger}_{l,\sigma} \tilde{c}_{l+1,\sigma} + \tilde{c}^{\dagger}_{l+1,\sigma} \tilde{c}_{l,\sigma} \right\} + J \sum_{l=1}^{N} \left\{ \mathbf{S}_l \cdot \mathbf{S}_{l+1} - \frac{1}{4} n_l n_{l+1} \right\}, \tag{1.3}$$

with $\tilde{c}_{l,\sigma} \equiv c_{l,\sigma}(1-n_{l,-\sigma})$, $n_l \equiv n_{l,\uparrow}+n_{l,\downarrow}$, $n_{l,\sigma} \equiv c^{\dagger}_{l,\sigma} c_{l,\sigma}$, $S^z_l \equiv \frac{1}{2}(n_{l,\uparrow} - n_{l,\downarrow})$, $S^+_l \equiv \tilde{c}^{\dagger}_{l,\uparrow} \tilde{c}_{l,\downarrow}$, and $S^-_l \equiv \tilde{c}^{\dagger}_{l,\downarrow} \tilde{c}_{l,\uparrow}$. The charge dynamics of $H_{t\text{-}J}$ as expressed by the dynamic structure factor

$$S_{nn}(q,\omega) = N^{-1} \sum_{l,n,\sigma,\sigma'} e^{-iqn} \int_{-\infty}^{+\infty} dt \times e^{i\omega t} \langle \tilde{c}^{\dagger}_{l,\sigma}(t) \tilde{c}_{l,\sigma}(t) \tilde{c}^{\dagger}_{l+n,\sigma'} \tilde{c}_{l+n,\sigma'} \rangle \tag{1.4}$$

is related, for weak exchange coupling, to the spin dynamics of H_{XXZ} as expressed by (1.2) near the XX case. The t-J model has its own spin dynamics, which will not be discussed here.

The continued-fraction analysis of dynamical properties presented here is based on the finite-size ground-state wave functions of the two model Hamiltonians (1.1) and (1.3). In the XXZ model we use systems with up to $N = 18$ spins and periodic boundary conditions. In the t-J model we consider systems with up to $N = 12$ sites and $N_e \equiv \sum_l n_l = N/2$ electrons. Here we use two types of boundary conditions: (i) $H_{t\text{-}J}$ with periodic boundary conditions in both the t term and the J term will be named the *c-cyclic* system. (ii) The alternative boundary condition, formally represented by an additive term to the t part of $H_{t\text{-}J}$,

$$H'_{t\text{-}J} = H_{t\text{-}J} + t \sum_{\sigma=\uparrow,\downarrow} \left\{ \tilde{c}^{\dagger}_{N,\sigma} \tilde{c}_{1,\sigma} + \tilde{c}^{\dagger}_{1,\sigma} \tilde{c}_{N,\sigma} \right\} \left[e^{i\pi N_e} + 1 \right], \tag{1.5}$$

introduces an extra minus sign to the hopping term involving sites 1 and N if the number of electrons is even. This will be called the *a-cyclic* system.[7] $H'_{t\text{-}J}$ with $J = 0$ in any state with all electrons up (or all down) is equivalent to H_{XXZ} with $J_z = 0$ and a periodic boundary condition.[2,8] The two kinds of boundary conditions give rise to two different level crossings in the weak-coupling regime. Awareness of these boundary effects is important for the finite-size analysis as we shall see.

A description in technical terms of the weak-coupling and strong-coupling regimes for the recursion method will be presented in Sec. II. Weak-coupling results for some infrared singularities produced by critical fluctuations and for the spectral-weight distribution in the dynamic structure factor $S_{zz}(\pi,\omega)$ and in the frequency-dependent spin autocorrelation function $S^{zz}(\omega)$ of the XXZ model will be discussed in Secs. III–VI. That discussion includes comparisons with exact results wherever possible, with strong-coupling results inferred from the same method, and with weak-coupling results derived by different methods. In the concluding Sec. VII we present weak-coupling results for the 1D t-J model and discuss them in comparison to the corresponding XXZ results.

II. WEAK-COUPLING AND STRONG-COUPLING REGIMES

The recursion method[9,10] as applied to the dynamic *correlation function* $\langle \phi_0 \mid A^{\dagger}(t) A \mid \phi_0 \rangle$ in the ground state of a given quantum many-body system can be based on an orthogonal expansion of the dynamical variable $A(t)$ (Liouvillian representation), or on an orthogonal expansion of the wave function $A(-t) \mid \phi_0\rangle$ (Hamiltonian representation).[11–14] The algorithms of both representations have been described in Ref. 1. They produce equivalent data, which are expressible (directly or indirectly) in terms of a sequence of continued-fraction coefficients, $\Delta_1, \Delta_2, \ldots$, for the *relaxation function*

$$c_0(z) = \cfrac{1}{z + \cfrac{\Delta_1}{z + \cfrac{\Delta_2}{z + \ldots}}} \,. \tag{2.1}$$

It is the Laplace transform of the symmetrized and normalized correlation function $\mathrm{Re}\langle \phi_0 \mid A^{\dagger}(t) A \mid \phi_0 \rangle / \langle \phi_0 \mid A^{\dagger} A \mid \phi_0 \rangle$. Its Fourier transform is the *spectral density* $\Phi_0(\omega)$ and can be recovered directly from (2.1):

$$\Phi_0(\omega) = \lim_{\varepsilon \to 0} 2\mathrm{Re}\left[c_0(\varepsilon - i\omega) \right]. \tag{2.2}$$

The Fourier transform of $\langle \phi_0 \mid A^{\dagger}(t) A \mid \phi_0 \rangle$ is the *structure function*

$$S(\omega) = 2\langle \phi_0 \mid A^{\dagger} A \mid \phi_0 \rangle \Phi_0(\omega) \Theta(\omega) \quad (T = 0). \tag{2.3}$$

In the context of the XXZ model, this becomes the dynamic structure factor (1.2) if we set $A = S^z_q$, and for $A = S^z_l$ it becomes the frequency-dependent spin autocorrelation function

$$S^{zz}(\omega) \equiv \int_{-\infty}^{+\infty} dt\, e^{i\omega t} \langle S^z_l(t) S^z_l \rangle = \int_{-\pi}^{+\pi} \frac{dq}{2\pi} S_{zz}(q,\omega). \tag{2.4}$$

These are the two quantities for which results will be presented and discussed in Secs. III–VI.

How do we recognize and distinguish the weak-coupling and strong-coupling regimes in the framework of the recursion method for a given dynamic quantity of interest? The relevant information is encoded in the Δ_k sequence as described in the following. In Fig. 1 we have plotted Δ_k versus k for the dynamic structure factor $S_{zz}(\pi,\omega)$ at $T = 0$ of H_{XXZ} at three different values of the anisotropy parameter (coupling constant).

For $J_z/J_\perp = 0$ (XX model) the Δ_k sequence is strictly linear with zero slope for $k \geq 2$. Convergence of Δ_k toward a finite value implies that the dynamically relevant

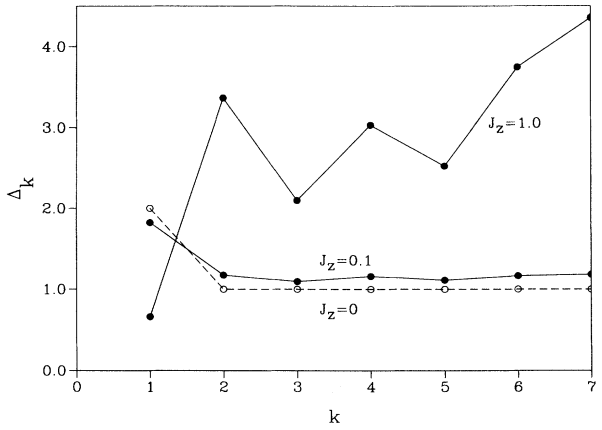

FIG. 1. Continued-fraction coefficients Δ_k vs k for the dynamic structure factor $S_{zz}(\pi,\omega)$ at $T=0$ of the 1D $s=1/2$ XXZ model (1.1) with energy scale $J_\perp=1$, and with couplings $J_z=0$ (free fermions), $J_z=0.1$ (weak-coupling regime), and $J_z=1.0$ (strong-coupling regime), as derived from the ground-state wave function for a chain with $N=16$ spins. The coefficients of the case $J_z=0$ are exact for the infinite system (Ref. 13), and those for $J_z\neq 0$ are nearly size independent as specified in Ref. 1. The coefficient Δ_7 for $J_z=0.1$ is already mildly affected by the crossover from zero growth to power-law growth.

spectrum is a band of finite width, in this case the two-particle spectrum of free lattice fermions. The constancy of Δ_k for $k\geq 2$ implies a particular spectral-weight distribution, which will be discussed in Sec. IV. For $J_z/J_\perp \neq 0$, the fermion interaction causes the continued-fraction coefficients to grow to infinity with the average growth described by some power law: $\Delta_k \sim k^\lambda$, $\lambda \geq 1$. This dramatic change in pattern signals the dynamic relevance of many-body collective modes with frequencies in a band of infinite width.[13,14] For sufficiently strong coupling, the power-law growth is manifest in the entire Δ_k sequence. In the context of Fig. 1 this is the case for $J_z/J_\perp=1$. For very weak coupling, on the other hand, the Δ_k sequence starts out with zero average growth as is illustrated by the case $J_z/J_\perp=0.1$. That sequence crosses over to power-law average growth for larger k (not shown in Fig. 1).

Naturally, the fermion coupling affects all continued-fraction coefficients Δ_k, but if it is very weak the impact on the first K_w coefficients is much more subtle than on the rest. The number K_w, which marks the crossover from zero growth to power-law growth, becomes smaller with increasing coupling strength. When K_w reaches zero, we are in the strong-coupling regime. The dynamical quantity is then governed by the full many-body spectrum. Under these circumstances the continued-fraction analysis must be carried out on the basis of the actual power-law growth of the Δ_k sequence. If, on the other hand, K_w is sufficiently large, we may proceed with just those coefficients Δ_k, $k=1,2,...,K_w$, which are still consistent with zero growth and carry out the continued-fraction analysis on that basis. This is what we call a weak-coupling approach within the framework of the recursion method. While the distinction between the weak-coupling and strong-coupling regimes of H_{XXZ} has its physical interpretation in the lattice-fermion representation of that model, the continued-fraction coefficients Δ_k for either regime are much more conveniently calculated in the spin representation.

The calculational scheme developed previously[13] and adopted here for the reconstruction of $T=0$ structure functions for H_{XXZ} and $H_{t\text{-}J}$ is based on an extrapolation of the dominant patterns which can be identified in the Δ_k sequences obtained from the recursion algorithm. The practical implementation of this scheme expresses the *exact relaxation function* $c_0(z)$ of (2.1) in terms of the known coefficients $\Delta_1,...,\Delta_K$ and an unknown termination function $\Gamma_K(z)$:

$$c_0(z)=\cfrac{1}{z+\cfrac{\Delta_1}{z+\ldots+\cfrac{\Delta_{K-1}}{z+\Delta_K\Gamma_K(z)}}}\,. \tag{2.5}$$

Now consider a *model relaxation function* $\bar{c}_0(z)$ determined via

$$\bar{c}_0(z)=\frac{1}{2\pi i}\int_{-\infty}^{+\infty} d\omega\,\frac{\bar{\Phi}_0(\omega)}{\omega-iz} \tag{2.6}$$

from some model spectral density $\bar{\Phi}_0(\omega)$ and express it, by continued-fraction expansion, in terms of K model coefficients $\bar{\Delta}_1,...,\bar{\Delta}_K$ and a model termination function $\bar{\Gamma}_K(z)$. The model spectral density $\bar{\Phi}_0(\omega)$ is to be chosen such that the model coefficients $\bar{\Delta}_1,...,\bar{\Delta}_K$ reproduce and extrapolate the dominant patterns of the recursion data $\Delta_1,...,\Delta_K$ optimally. The *reconstructed relaxation function* $\tilde{c}_0(z)$ is then obtained by substituting the known, matching termination function $\bar{\Gamma}_K(z)$ for the unknown function $\Gamma_K(z)$ in (2.5).

In Ref. 1 we have introduced two model spectral densities which are suitable for strong-coupling applications, including the reconstruction of $S_{zz}(\pi,\omega)$ from the Δ_k sequence labeled $J_z/J_\perp=1.0$ in Fig. 1. In the weak-coupling applications presented here, the Δ_k sequences exhibit different patterns, which call for different types of model spectral densities. Two such functions will be introduced in Secs. IV and V.

III. WEAK-COUPLING ANALYSIS OF INFRARED SINGULARITIES

Some aspects of the critical fluctuations in the ground state of H_{XXZ} for $-1<J_z/J_\perp\leq 1.0$ are described by a power-law infrared singularity in the dynamic structure factor $S_{zz}(q,\omega)$ at $q=\pi$,[15]

$$S_{zz}(\pi,\omega)\sim\omega^{\beta_z}, \tag{3.1}$$

with the exponent explicitly known as a function of the coupling constant,

$$\beta_z=\frac{1}{\theta}-2,\qquad \theta=1-\frac{1}{\pi}\arccos\left(\frac{J_z}{J_\perp}\right). \tag{3.2}$$

Here we demonstrate a general method by which this singularity exponent can be derived from a small number of continued-fraction coefficients Δ_k in the weak-coupling regime and discuss the results in conjunction with those previously obtained from a strong-coupling exponent analysis.[1] In Sec. VII we shall apply the same weak-coupling exponent analysis to the t-J model, for which exact results are not known. The exact expression

$$S_{zz}(q,\omega) = \frac{2\Theta(\omega - J_\perp \sin q)\,\Theta(2J_\perp \sin(q/2) - \omega)}{\sqrt{4J_\perp^2 \sin^2(q/2) - \omega^2}} \tag{3.3}$$

at $J_z/J_\perp = 0$ for the dynamic structure factor was first derived from a two-particle Green's function for free lattice fermions.[3,16] For $q = \pi$ it can be recovered with little effort[13] from the Δ_k sequence

$$\Delta_1 = 2J_\perp^2, \quad \Delta_2 = \Delta_3 = \cdots = J_\perp^2, \tag{3.4}$$

obtained by the recursion method and shown in Fig. 1 (open circles).

In the weak-coupling regime, $|J_z/J_\perp| \ll 1$, the fermion interaction produces two kinds of deviations of the Δ_k's from the reference sequence (3.4). (i) The new sequence tends to converge toward a different value $\Delta_\infty^{(w)}$ as k increases toward K_w. (ii) The Δ_{2k} and Δ_{2k-1} approach $\Delta_\infty^{(w)}$ from opposite sides. Both effects are conspicuous for $J_z/J_\perp = 0.1$ in Fig. 1. All deviations from (3.4) switch direction with the sign of the coupling constant $J_z/J_\perp$.

The shift of the pseudoasymptotic value $\Delta_\infty^{(w)}$ [effect (i)] describes the renormalized bandwidth ω_0 of the particle-hole continuum of lattice fermions via the relation[13]

$$\Delta_\infty^{(w)} = \frac{1}{4}\omega_0^2. \tag{3.5}$$

For the case at hand, the value $\Delta_\infty^{(w)}$ has been determined as the average of $\Delta_2, \ldots, \Delta_5$. The resulting band-edge frequency ω_0 (for $|J_z/J_\perp| \leq 0.1$) reproduces very accurately the exactly known boundary

$$\varepsilon_U(q) = \frac{\pi J_\perp \sin\vartheta}{\vartheta} \sin\frac{q}{2}, \qquad \cos\vartheta = \frac{J_z}{J_\perp} \tag{3.6}$$

at $q = \pi$ of the spinon continuum.[17] Explicit results in comparison will be shown in Sec. VII.

The alternating approach of the Δ_k toward $\Delta_\infty^{(w)}$ [effect (ii)] describes the infrared singularity (3.1) in the dynamic structure factor. For a truly convergent Δ_k sequence, the exponent of the infrared singularity, $\sim \omega^\gamma$, is determined by the leading term of the large-k asymptotic expansion[18]

$$\Delta_k = \Delta_\infty \left[1 - (-1)^k \frac{\gamma}{k} + \cdots\right]. \tag{3.7}$$

The exponent value γ is then most conveniently extracted by analyzing the sequence

$$\gamma_k = (-1)^k k \left[1 - \frac{\Delta_k}{\Delta_\infty}\right], \tag{3.8}$$

which converges toward γ for $k \to \infty$.[13] Such an analysis can still be carried out for the finite sequences $\Delta_1, \ldots, \Delta_{K_w}$ available for our weak-coupling analysis of the exponent β_z.

Two such sequences (3.8), $\beta_z^{(k)}$ vs $1/k$, are shown in the upper inset to Fig. 2. For the determination of the infrared exponent from that sequence we propose two alternative schemes. (i) *Averaging*: The exponent β_z is assigned the mean value of an even number of successive $\beta_z^{(k)}$'s. These data points are shown as open squares in the main plot. (ii) *Extrapolation*: The trends indicated by the $\beta_z^{(k)}$'s for even k and odd k are extended linearly to $k \to \infty$ as marked by dashed lines in the upper inset. The average of the two intersection points with the vertical axis is taken as the data point for β_z in the main plot (open circles).

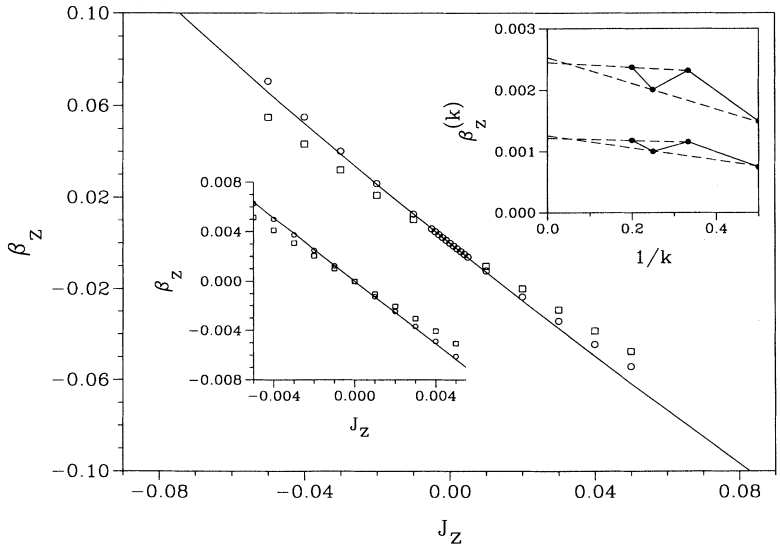

FIG. 2. J_z dependence of the infrared exponent β_z pertaining to the dynamic structure factor $S_{zz}(\pi,\omega)$ at $T = 0$ of the 1D $s = 1/2$ XXZ model (1.1) with $J_\perp = 1$. In the main plot the solid line represents the exact result (3.2), and the open symbols the results of our weak-coupling analysis based on the nearly-size-independent continued-fraction coefficients $\Delta_1, \ldots, \Delta_5$ computed for a system of $N = 18$ spins. The squares result from the averaging method and the circles from the extrapolation method as described in the text. The lower inset is a blowup of the main plot near $J_z = 0$. The upper inset illustrates the extrapolation procedure used for the exponent sequences (3.8) at $J_z = -0.003$ (top), $J_z = -0.001$ (bottom) as described in the text.

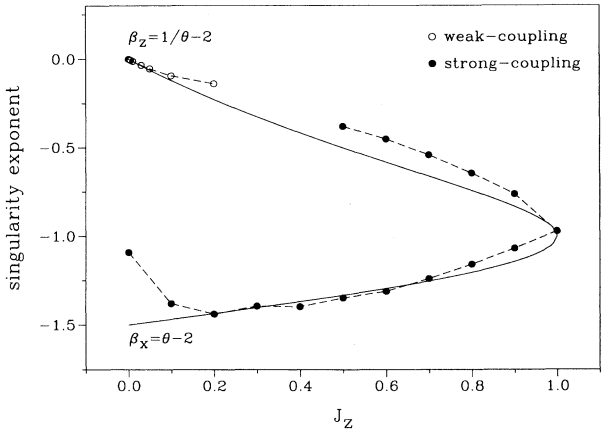

FIG. 3. J_z dependence of the infrared-singularity exponents β_μ, $\mu = x, z$ for $S_{\mu\mu}(\pi,\omega)$ at $T = 0$ of the 1D $s = 1/2$ XXZ model (1.1) with $J_\perp = 1$. The solid circles represent the results derived, via strong-coupling analysis as explained in Ref. 1, from a number of nearly-size-independent Δ_k's computed for systems with up to $N = 18$ spins. The exact results are shown as solid lines. The open circles represent the weak-coupling results for β_z as in Fig. 2 but over an extended range of (positive) coupling strengths.

Both sets of data points display a smooth dependence on $J_z/J_\perp$ over the interval of anisotropy shown. Also shown in the main plot is the exact $J_z/J_\perp$ dependence (3.2) of the exponent β_z (solid line). Note that the line through the circles has the correct slope near the free-fermion limit ($J_z/J_\perp = 0$), whereas the line through the squares has a somewhat different slope. The lower inset shows the center region of the main plot on a magnified scale. The conclusion is that the weak-coupling continued-fraction analysis of the infrared exponent β_z is fairly reliable. In this instance, extrapolation improves the accuracy significantly over that of averaging.

In Ref. 1 we have already determined the exponent β_z in the strong-coupling regime $0.5 \leq J_z/J_\perp \leq 1.0$ of the XXZ antiferromagnet. In Δ_k sequences with nonzero growth, such as shown in Fig. 1 for $J_z/J_\perp = 1.0$, the information on the infrared exponent is encoded differently and must, therefore, be extracted by different means. In Fig. 3 (upper branch) we show those strong-coupling results (solid circles) together with the weak-coupling results at $0 \leq J_z/J_\perp \leq 0.2$ (open circles) and the exact results (solid line) for the exponent β_z. The gap between the two sets of results marks the crossover region where no meaningful continued-fraction exponent analysis can be carried out on the basis of the limited number of known coefficients. The lower branch depicts the exact exponent $\beta_x = \theta - 2$ of the dynamic structure factor $S_{xx}(\pi,\omega)$ and the result from Ref. 1 of the continued-fraction analysis. For this function, the entire parameter range shown belongs to the strong-coupling regime.[19]

IV. DYNAMIC STRUCTURE FACTOR $S_{zz}(\pi,\omega)$

The goal here is to determine the line shapes of $S_{zz}(q,\omega)$ at the critical wave number $q = \pi$ in the weak-coupling regime of H_{XXZ}, specifically the deviations from the exact result (3.3) caused by the fermion interaction in the framework of a weak-coupling continued-fraction analysis.

In the insets to Fig. 4 we have plotted six Δ_k's for (a) two cases with weak repulsive coupling ($J_z/J_\perp > 0$) and (b) one case with weak attractive coupling ($J_z/J_\perp < 0$) along with the sequence (3.4) as a reference. The two dominant effects of the interaction on the Δ_k's have already been identified in Sec. III and analyzed quantitatively in terms of a renormalized bandwidth ω_0 and an infrared singularity exponent γ, both of which depend continuously on $J_z/J_\perp$. These two quantities alone contain already a fair amount of information on the line shapes. Since both quantities have been extracted from the Δ_k's, it is legitimate to employ them as parameters with fixed values $\omega_0 \simeq \varepsilon_U(\pi)$, $\gamma \simeq \beta_z$ in the model spectral density to be used for the weak-coupling continued-fraction analysis for this situation. A simple function which incorporates these two parameters is the following:

$$\bar{\Phi}_0(\omega) = \frac{\pi}{\omega_0}(1+\gamma)\mid \omega/\omega_0 \mid^\gamma \Theta(\omega_0 - \mid \omega \mid). \tag{4.1}$$

The associated model continued-fraction coefficients are then also functions of ω_0 and γ:

$$\Delta_k = \begin{cases} \dfrac{\omega_0^2 k^2}{(2k-1+\gamma)(2k+1+\gamma)} & (\text{even } k), \\ \dfrac{\omega_0^2 (k+\gamma)^2}{(2k-1+\gamma)(2k+1+\gamma)} & (\text{odd } k). \end{cases} \tag{4.2}$$

The reconstruction with termination at level $K = 5$ based on this model spectral density yields the curves for $J_z/J_\perp = 0.1$, 0.2, and -0.1 in Fig. 4.

In the antiferromagnetic case ($J_z/J_\perp > 0$), we observe an increase in bandwidth and the emergence of an infrared divergence. These are effects previously seen in the Δ_k sequence and then incorporated into the termination function via (4.1). But near the band edge the termination function is unbiased with respect to any structures that might emerge from the weak-coupling reconstruction. Here the model spectral density is flat and drops to zero discontinuously. The reconstructed dynamic structure factor $S_{zz}(\pi,\omega)$ as shown in Fig. 4(a) exhibits a softening of the square-root divergence at the band edge as $J_z/J_\perp$ increases from zero. At $J_z/J_\perp = 0.2$ the spectral enhancement has all but disappeared. That trend combined with the strengthening of the infrared divergence connects perfectly with the strong-coupling result for $J_z/J_\perp = 1.0$ presented in Fig. 4(a) of Ref. 1.

In the ferromagnetic case ($J_z/J_\perp < 0$), the bandwidth shrinks and a cusp singularity develops at $\omega = 0$ as shown in Fig. 4(b). This is in conformance with the parameter values $\omega_0 \simeq \varepsilon_U(\pi)$, $\gamma \simeq \beta_z$ in (4.1) as inferred from the Δ_k sequence shown in the inset. Unlike in the antiferromagnetic case, the spectral enhancement at the band edge stays strongly peaked. Furthermore, a discrete state is observed to split off the upper boundary $\varepsilon_U(\pi)$ of the spinon continuum. It is represented in $S_{zz}(\pi,\omega)$ by a δ function separating from the band edge at $J_z/J_\perp = 0^-$.[20] This discrete state is readily identified as belonging to the

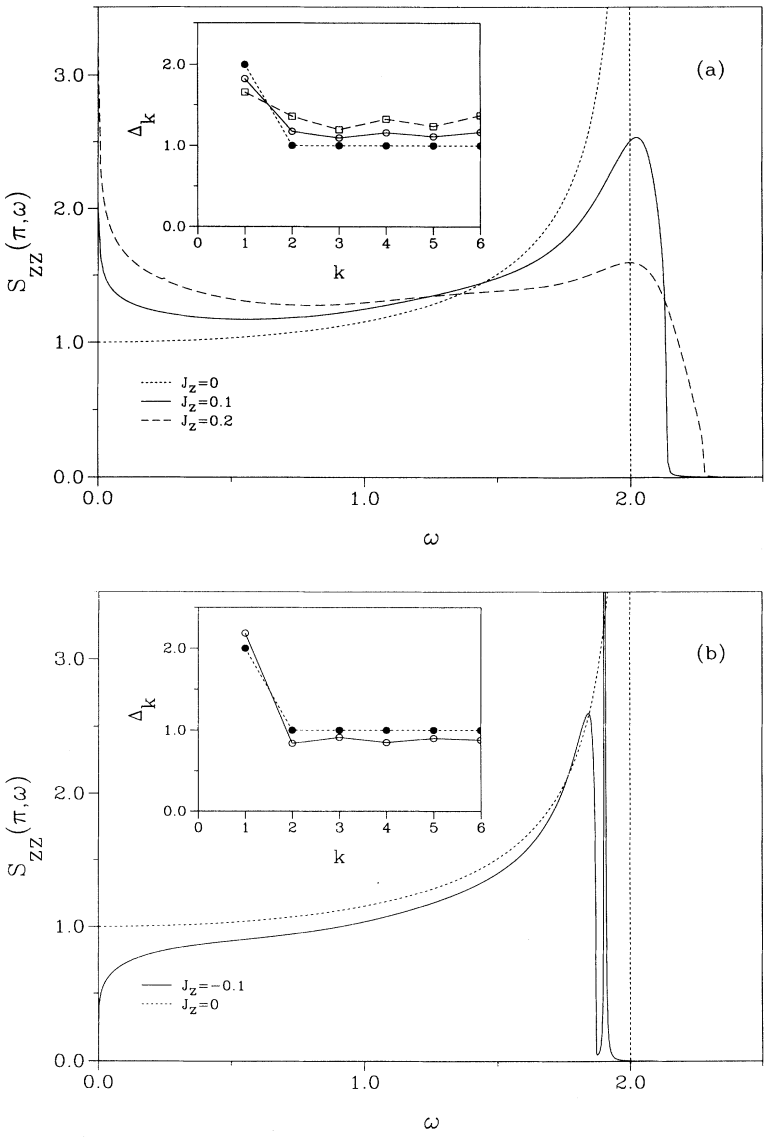

FIG. 4. Dynamic structure factor $S_{zz}(\pi,\omega)$ at $T=0$ of the 1D $s=1/2$ XXZ model (1.1) with (a) antiferromagnetic coupling ($J_\perp=1, J_z\geq 0$) and (b) ferromagnetic coupling ($J_\perp=1, J_z\leq 0$). The short-dashed curve in each plot represents the exact result (3.3) for the XX case ($J_z=0$). The remaining curves are the results of a weak-coupling reconstruction as described in the text. The insets show the Δ_k sequences for the same three cases. The coefficients shown are exactly size independent for $J_z=0$ and nearly size independent for $J_z\neq 0$. The latter have been extracted from the ground-state wave function of a system with $N=16$ spins.

first branch of bound states, which are part of the exactly known spectrum of low-lying excitations of H_{XXZ}.[21] The exact excitation energy with which the pole position in Fig. 4(b) must be compared is $\varepsilon_1(\pi)$, where

$$\varepsilon_1(q)=\frac{\pi J_\perp \sin\vartheta}{\vartheta\,\sin y}\sin\frac{q}{2}\sqrt{\sin^2\frac{q}{2}+\sin^2 y\cos^2\frac{q}{2}}, \qquad (4.3)$$

and $y=\pi(1-\vartheta)/2\vartheta$. The agreement is near perfect for $|\,J_z/J_\perp\,|\leq 0.1$.

In order to gain some insight into how the bound state contribution to $S_{zz}(\pi,\omega)$ at $J_z/J_\perp<0$ is encoded in the continued-fraction coefficients of that function, we consider the model sequence

$$\bar{\Delta}_1=2\Delta+\Gamma,\quad \bar{\Delta}_2=\bar{\Delta}_3=\cdots\equiv\Delta. \qquad (4.4)$$

With $\Gamma\propto J_z/J_\perp$ and $\Delta-J_\perp^2\propto J_z/J_\perp$, as inferred empirically from our data, it describes the predominant pattern of the weak-coupling Δ_k sequences displayed in the insets to Fig. 4. For $\Gamma>0$ the associated model relaxation function

$$\bar{c}_0(z)=\frac{1}{z+(2\Delta+\Gamma)\Gamma_1(z)}, \qquad (4.5)$$

with $\Gamma_1(z)=[z+\Delta\Gamma_1(z)]^{-1}$, exhibits a pair of isolated poles. The model spectral density $\bar{\Phi}_0(\omega)$ inferred from (4.5) via (2.2) is then the sum of a continuous part

$$\bar{\Phi}_0^c(\omega)=\frac{\left(1+\frac{\Gamma}{2\Delta}\right)\sqrt{4\Delta-\omega^2}\;\Theta(4\Delta-\omega^2)}{4\Delta\left(1+\frac{\Gamma}{2\Delta}\right)^2-\left(1+\frac{\Gamma}{\Delta}\right)\omega^2} \qquad (4.6)$$

and a discrete part

$$\bar{\Phi}_0^p(\omega)=\frac{\pi}{2}\frac{|\,\Gamma\,|+\Gamma}{4(\Delta+\Gamma)}\left[\delta(\omega-\omega_p)+\delta(\omega+\omega_p)\right], \qquad (4.7)$$

with

$$\omega_p = \frac{2\Delta+\Gamma}{\sqrt{\Delta+\Gamma}} = 2\sqrt{\Delta}\left(1+\frac{1}{8}\frac{\Gamma^2}{\Delta^2}+\cdots\right). \quad (4.8)$$

The absence of the discrete part for $\Gamma < 0$ is in agreement with the results for the reconstructed function $S_{zz}(\pi,\omega)$. In this application the presence of a discrete state in the weak-coupling results of Fig. 4 depends principally on the displacement of the first coefficient relative to the remaining ones, which are nearly constant.

V. SPIN AUTOCORRELATION FUNCTION $S^{zz}(\omega)$

From the frequency-dependent spin autocorrelation function (2.4), subjected to its own weak-coupling continued-fraction analysis, we can expect to gain further insight into the $T = 0$ dynamics of H_{XXZ}. At the same time, the results from such an analysis can be tested against some exactly known spectral properties and against the implications of the results reported in Sec. IV for the dynamic structure factor $S_{zz}(q,\omega)$.

For $J_z/J_\perp = 0$, the function $S^{zz}(\omega)$ can be obtained by integration from the exactly known dynamic structure factor (3.3). The result is expressible in terms of elliptic functions as follows:[22]

$$S^{zz}(\omega) = \frac{4}{\pi J_\perp} F\left[\arcsin\left(\left\{\frac{1}{2}\left[1-(1-\omega^2/J_\perp^2)^{\frac{1}{2}}\right]\right\}^{\frac{1}{2}}/k\right), k\right]\Theta(\omega)\Theta(J_\perp-\omega) + \frac{2}{\pi J_\perp}K(k)\,\Theta(\omega-J_\perp)\Theta(2J_\perp-\omega), \quad (5.1)$$

with $k = (1-\omega^2/4J_\perp^2)^{1/2}$. This function is plotted as dashed line in Fig. 5. It grows linearly from zero at $\omega = 0$, has a square-root cusp at $\omega = J_\perp$, and drops back to zero discontinuously at $\omega = 2J_\perp$. Here we use a symmetrized version of (5.1) as the model spectral density for the reconstruction of $S^{zz}(\omega)$ at small positive and negative couplings $J_z/J_\perp$. The associated model $\bar{\Delta}_k$ sequence can be derived from the frequency moments of (5.1).[23,24]

As in the applications of Sec. IV, the predominant effect of $J_z/J_\perp \neq 0$ on the Δ_k's is an overall shift, which is related to the renormalized bandwidth (3.6) of the spinon continuum. For the present line-shape analysis we have eliminated this effect by a simple rescaling of the frequency: $\omega' = 2\omega/\varepsilon_U(\pi)$, $\Delta_k' = 4\Delta_k/\varepsilon_U^2(\pi)$. For the weak-coupling reconstruction of $S^{zz}(\omega)$ at $J_z/J_\perp \neq 0$, we use the coefficients $\Delta_1,\ldots,\Delta_5$ extracted from the ground-state wave function of a system with $N = 16$ spins by means of the recursion method. These coefficients are subject to only very weak finite-size effects, which have negligible impact on the results.[25] The reconstructed function $S^{zz}(\omega)$ for the two cases $J_z/J_\perp = \pm 0.04$ is shown as solid lines in the main plot of Fig. 5. The impact of a weak fermion coupling is strongest near the upper boundary of the spinon continuum. For $J_z/J_\perp > 0$ the spectral weight near $\omega' = 2$ is suppressed considerably. This is consistent with the observation made in Sec. IV that the density-of-states divergence in $S_{zz}(\pi,\omega)$ at $\omega = \varepsilon_U(\pi)$ is offset by vanishing matrix elements.

For $J_z/J_\perp < 0$, on the other hand, the discontinuity at the band edge has transformed into a divergent endpoint singularity at a frequency slightly above $\omega' = 2$. A bound-state branch $\varepsilon_1(q)$ with a smooth maximum (4.3) at $q = \pi$ and smoothly varying spectral weight would

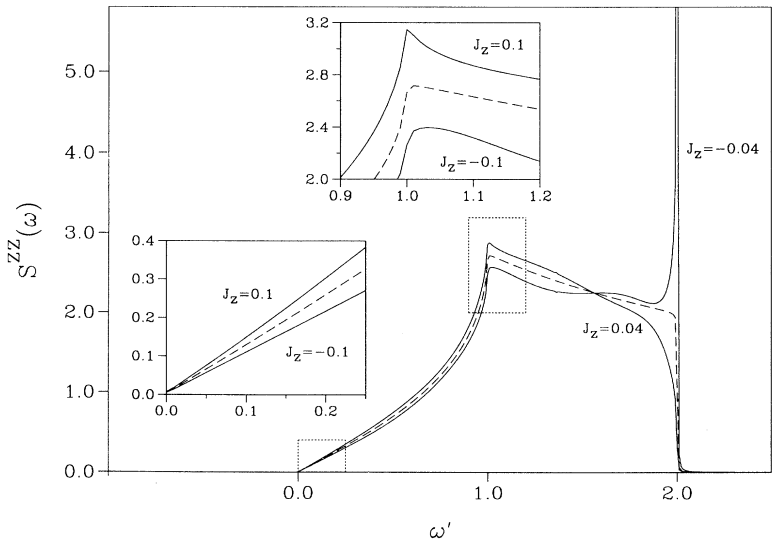

FIG. 5. Spin autocorrelation function $S^{zz}(\omega)$ at $T = 0$ of the 1D $s = 1/2$ XXZ model (1.1) with $J_\perp = 1$. The dashed curve represents the exact result (5.1) for the XX case ($J_z = 0$). The solid curves are the results of a weak-coupling reconstruction as described in the text. The insets show parts of the corresponding curves on expanded scales for somewhat larger coupling strengths. Bandwidth renormalization effects have been eliminated by employing the rescaled frequency ω' as described in the text.

indeed produce a square-root divergence at precisely the frequency where $S_{zz}(\pi,\omega)$ has a discrete state.

At $\omega' \simeq 1$, the deviations from the dashed curve are in opposite directions compared to those at $\omega' \simeq 2$. The cusp grows sharper and higher for $J_z/J_\perp > 0$ and becomes round and inconspicuous for $J_z/J_\perp < 0$. These trends are further amplified for $J_z/J_\perp = \pm 0.1$ as shown in the upper inset. They suggest that the spectral weight in $S_{zz}(q,\omega)$ along the lower spinon continuum boundary $\varepsilon_L(q) = \varepsilon_U(2q)/2$ is enhanced for $J_z/J_\perp > 0$ and suppressed for $J_z/J_\perp < 0$ as we have, in fact, observed for $q = \pi$ in Fig. 4. According to this interpretation, the same trends should then persist over the frequency interval $0 \leq \omega' \leq 1$ as is indeed the case.

At small frequencies, the linear behavior at $J_z/J_\perp = 0$ should transform into a cusp singularity of the form $S^{zz}(\omega) \sim \omega^{\beta_z+1}$ with β_z from (3.2). The curves in Fig. 5 (see also the lower inset) give no hint of such a change. Unlike for $S_{zz}(\pi,\omega)$ we have not been able to extract the $J_z/J_\perp$ dependence of the infrared exponent $\beta_z + 1$ from the first few Δ_k's and, therefore, have had no legitimacy to incorporate that singularity into the model spectral density.[26] The gradual deviations of the reconstructed function $S^{zz}(\omega)$ from the dashed line for increasing values of $J_z/J_\perp$ as seen in Fig. 5 connect well with the result of a strong-coupling continued-fraction analysis presented in Ref. 1: The spectral weight at small frequencies continues to build up. The cusp at $\omega' = 1$ grows into a divergence, while the shoulder at $\omega' = 2$ continues to weaken. But unlike the results of Fig. 5, the strong-coupling analysis yields nonzero spectral weight beyond the frequency $\omega' = 2$.

VI. OTHER WEAK-COUPLING APPROACHES

The dynamic structure factor $S_{zz}(q,\omega)$ at $T = 0$ of H_{XXZ} was previously investigated by means of a Hartree-Fock analysis in the lattice fermion representation,[4,27,28] which is an alternative and independent weak-coupling approach. Even though it is very different in nature from the weak-coupling continued-fraction analysis, it turns out that the two methods yield results that are remarkably consistent and accurate:

(i) The dynamically relevant excitation spectrum of the Hartree-Fock result for $S_{zz}(q,\omega)$ is a renormalized two-particle spectrum, in agreement to $O(J_z/J_\perp)$ with the exactly known spinon continuum as was the renormalized bandwidth in the continued-fraction analysis. (ii) The Hartree-Fock analysis predicts a discrete state above the continuum for $J_z/J_\perp < 0$ as did the continued-fraction analysis.[29] In both weak-coupling approaches the gap between this state and the edge of the continuum grows quadratically in $J_z/J_\perp$ for fixed q, in agreement with the exactly known spectral properties.[17,21] (iii) Both methods predict that the spectral weight of the discrete state increases linearly with $J_z/J_\perp$. (iv) Both types of analysis produce very similar line shapes for weak (positive and negative) couplings. (v) In the Hartree-Fock result for $S_{zz}(\pi,\omega)$, the infrared singularity is logarithmic in nature. If it is interpreted as the logarithmic correction to a power-law singularity, the exponent β_z is correct to $O(J_z/J_\perp)$ as was the result of the continued-fraction analysis.

The continuum analysis of $S_{zz}(q,\omega)$ on the level of the Luttinger model (without umklapp terms in the fermion interaction) shares some features with the two weak-coupling approaches discussed previously:[15,30] It produces an exponent β_z that is correct to $O(J_z^2/J_\perp^2)$, and it predicts a spin-wave velocity that agrees to $O(J_z/J_\perp)$ with the spinon continuum boundaries $\varepsilon_U(q)$ and $\varepsilon_L(q)$ for small q.

It is appropriate to mention, in this context, an explicit expression for the dynamic structure factor $S_{zz}(q,\omega)$ of the 1D $s = 1/2$ XXZ antiferromagnet in the critical regime ($0 \leq J_z/J_\perp \leq 1$) that was proposed on the basis of numerical finite-chain results and sum rule arguments:[31]

$$S_{zz}(q,\omega) = A_z \frac{\Theta(\omega - \varepsilon_L(q))\Theta(\varepsilon_U(q) - \omega)}{[\omega^2 - \varepsilon_L^2(q)]^{\frac{\beta_z}{2}} \; [\varepsilon_U^2(q) - \omega^2]^{\frac{1-\beta_z}{2}}}, \quad (6.1)$$

with β_z from (3.2) and a $J_z/J_\perp$-dependence factor A_z. It was designed to provide a reasonably accurate description of the spectral-weight distribution within the spinon continuum. Expression (6.1) connects smoothly with the exact result (3.3) for $J_z/J_\perp = 0$ and exhibits the correct singularity at $q \simeq \pi$ over the entire critical regime. Moreover, the line shapes produced by the weak-coupling results presented in Sec. IV agree well with the result (6.1) for $| J_z/J_\perp | \ll 1$. Expression (6.1) for $J_z/J_\perp = 1$ was recently used to interpret inelastic neutron scattering experiments on the quasi-1D antiferromagnetic compound $KCuF_3$.[32]

VII. CHARGE DYNAMICS OF THE 1D t-J MODEL

A. Finite-size ground state

Whereas H_{XXZ} has a nondegenerate ground state at $| J_z/J | < 1$ for all even N, the ground state of $H_{t\text{-}J}$ is highly spin degenerate at $J/t = 0$.[33] The (isotropic) exchange coupling splits it into $(2S_T + 1)$-fold degenerate spin multiplets, where S_T is the total spin. The ground-state degeneracy is thus completely removed if the lowest-lying level is a singlet ($S_T = 0$). This is expected to be the case for $J/t > 0$, while, at $J/t < 0$, one expects the ground state to be the multiplet with all electrons ferromagnetically aligned ($S_T = N_e/2$). In reality the situation is more subtle. For finite $N_e = N/2$, level crossings occur at $J/t \neq 0$, and they depend on the boundary conditions.

Consider a very small system, $N_e = 2$ electrons on $N = 4$ sites. The J/t dependence of the complete spectrum is displayed in Fig. 6 for both a-cyclic and c-cyclic boundary conditions. The solid lines are singlets ($S_T = 0$) and the dashed lines triplets ($S_T = 1$).[34] The observations which remain relevant for larger systems are the following: (i) The a-cyclic ground state is a triplet for all $J/t < 0$ and the c-cyclic ground state a singlet for all $J/t > 0$. (ii) Level crossings involving the ground

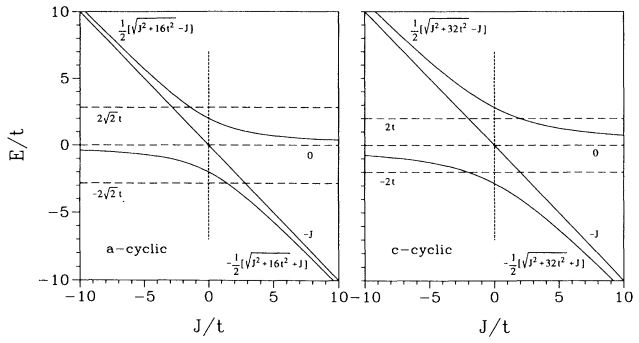

FIG. 6. Dependence on the coupling constant of the complete spectrum of $H_{t\text{-}J}$ with $N_e = 2$ electrons on $N = 4$ sites for a-cyclic and c-cyclic boundary conditions. The singlets ($S_T = 0$) are denoted by solid lines and the triplets ($S_T = 1$) by dashed lines.

state occur at small positive J/t in the a-cyclic system and small negative J/t in the c-cyclic system.

In the system of size $N = 2N_e = 12$, on which our continued-fraction analysis is based, we observe the following: The c-cyclic ground state is a singlet at $J/t > 0$ throughout the weak-coupling regime.[35] At $J/t = 0$ this singlet is degenerate with the S_T multiplets for $S_T = 1, \ldots, N_e/2 - 1$. The $S_T = N_e/2$ multiplet has a higher energy. At small negative J/t the $S_T < N_e/2$ multiplets split apart with the singlet again at the bottom. The singlet remains the ground state until it crosses (at $J/t \simeq -2$) the J/t-independent level of the $S_T = N_e/2$ multiplet.

Conversely, the ground state of the a-cyclic system is the ferromagnetically ordered $S_T = N_e/2$ multiplet for all $J/t < 0$. This state does not change directly into a singlet at $J/t = 0$. We find an $S_T = 1$ ground state over the entire $J/t > 0$ weak-coupling regime accessible to our numerical analysis,[35] and a transition to the $S_T = 0$ ground state at $J/t \simeq 1.2$. We conclude that the physical properties of the 1D t-J model in the weak-coupling regime are represented in a finite system most faithfully, if we impose a-cyclic boundary conditions for $J/t < 0$ and c-cyclic boundary conditions at $J/t > 0$.

B. Continued-fraction analysis of $S_{nn}(q,\omega)$

For zero exchange coupling ($J/t = 0$) and a quarter-filled band, the charge dynamic structure factor $S_{nn}(q,\omega)$ at $T = 0$ of $H_{t\text{-}J}$ is the same expression (except for trivial modifications) as the spin dynamic structure factor $S_{zz}(q,\omega)$ of H_{XXZ} for $J_z/J_\perp = 0$:

$$S_{nn}(q,\omega)_{t\text{-}J} = S_{zz}(q,\omega)_{XXZ} + \pi^2\delta(q)\delta(\omega), \qquad (7.1)$$

with $J_\perp = 2t$ in (3.3). The effect of a spin coupling, $| J/t | \ll 1$, on the charge dynamics of $H_{t\text{-}J}$ can then be investigated by the same weak-coupling continued-fraction analysis previously employed to study the effects of anisotropy in the spin dynamics of H_{XXZ} for $| J_z/J_\perp | \ll 1$. The results for the two models exhibit many similarities, but there are some important differences. Both aspects are most effectively presented in the form of comparative plots of several key quantities.

One consequence of the ground-state degeneracy at $J/t = 0$ is that the $T = 0$ dynamical properties of $H_{t\text{-}J}$ do not vary smoothly with J/t across the point of zero coupling. This is in sharp contrast to the XXZ model, where the point $J_z/J_\perp = 0$ is nonsingular. The regular $J_z/J_\perp$ dependence of the XXZ dynamics and the singular J/t dependence of the t-J dynamics at the respective free-fermion points are also present in the data extracted by the recursion method from the finite-size ground-state wave function. Figure 7 shows the dependence on the coupling constant of the first two continued-fraction coefficients Δ_1 and Δ_2 for $S_{zz}(\pi,\omega)$ of H_{XXZ} (left) and for $S_{nn}(\pi,\omega)$ of $H_{t\text{-}J}$ (right). Near the point of zero interaction, the Δ_k's depend linearly on the coupling constant in both models. For the following weak-coupling

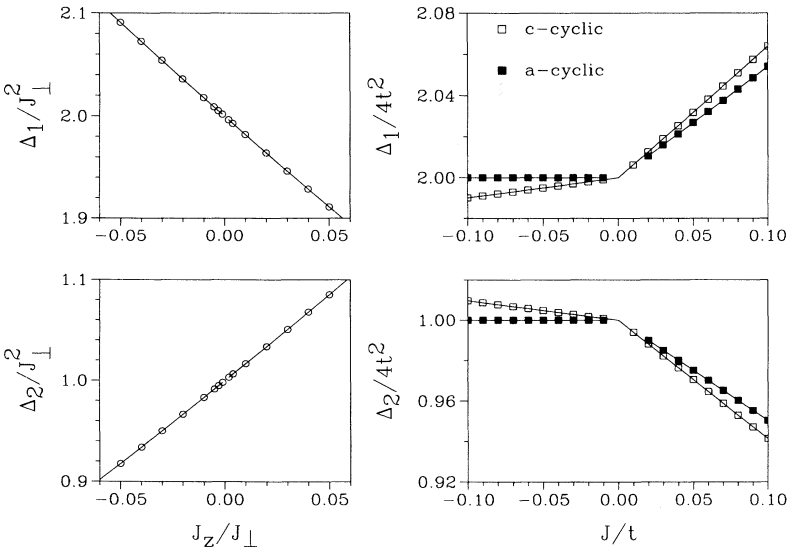

FIG. 7. Dependence on the coupling constant of the continued-fraction coefficients Δ_1 (top) and Δ_2 (bottom) for the dynamic structure factors $S_{zz}(\pi,\omega)$ of H_{XXZ} (left) and $S_{nn}(\pi,\omega)$ of $H_{t\text{-}J}$ (right). The XXZ data (circles) have been obtained by the recursion method for a system with 16 spins and periodic boundary condition, and the t-J data (squares) for a system with $N_e = 6$ electrons on a lattice with $N = 12$ sites with a-cyclic and c-cyclic boundary conditions.

continued-fraction analysis of the t-J dynamics, we shall use the a-cyclic system at $J/t < 0$ and the c-cyclic system at $J/t > 0$.

C. Renormalized bandwidth of particle-hole excitations

From the average J/t dependence of the coefficients $\Delta_2, \ldots, \Delta_5$ we can determine a renormalized bandwidth for the dynamically relevant charge excitations in the weak-coupling regime. The method has been described in Sec. III. We have used it there to determine the renormalized bandwidth of the spin excitations which are dynamically relevant for $S_{zz}(q,\omega)$. In both H_{XXZ} (fermion representation) and $H_{t\text{-}J}$, these excitations are of the particle-hole type.

The results of the bandwidth analysis for both models are displayed in the inset to Fig. 8. The $J_z/J_\perp$ dependence of the XXZ bandwidth as represented by the circles is perfectly regular in the noninteracting limit and reproduces the spinon continuum boundary $\varepsilon_U(\pi)$ (solid line) very accurately. The J/t dependence of the renormalized t-J bandwidth is represented by the squares in the same plot. The solid squares reflect the fact that a ferromagnetic exchange coupling has no effect on the charge dynamics. The open squares fall onto an inclined straight line (shown dashed) which extrapolates toward the free-electron bandwidth $\omega_0 = 2t$ at $J/t = 0$.

In the XXZ model, the ratio of the spin velocity $v_s = [d\varepsilon_U(q)/dq]_{q=0}$ to the spinon bandwidth $\omega_0 = \varepsilon_U(\pi)$ is independent of $J_z/J_\perp$, $2v_s/\omega_0 = 1$, as can be derived from the continuum boundary (3.6). Under the assumption that the same relationship holds between the charge velocity v_c and the particle-hole bandwidth ω_0 in the t-J model, $2v_c/\omega_0 = 1$, we can compare our result

$$\omega_0/2t \simeq 2 - 0.45J/t, \tag{7.2}$$

derived from the data displayed in Fig. 8, with the result $v_c/t \simeq 2 - 0.46J/t$ inferred from the approximately linear dependence of the charge velocity on the coupling constant between the noninteracting case J/t=0 and the supersymmetric case $J/t = 2$ as reported by Ogata *et al.*[36] on the basis of a numerical analysis of systems with up to $N = 16$ sites.

D. Infrared singularity in $S_{nn}(\pi,\omega)$

There exists overwhelming evidence that the ground state of $H_{t\text{-}J}$ is a Luttinger liquid between $J/t = 0$ and some point beyond $J/t = 2$, before phase separation starts to take place. One characteristic signature of this critical ground state is the infrared singularity in the charge dynamic structure factor:

$$S_{nn}(\pi,\omega) \sim \omega^{\beta_n}. \tag{7.3}$$

Unlike the exponent β_z in (3.1) of H_{XXZ}, the exponent β_n is not exactly known. Therefore, it is useful to determine its J/t dependence from the continued-fraction coefficients $\Delta_2, \ldots, \Delta_5$ by the same two methods, *averaging* and *extrapolation* , as used for β_z in Sec. III.

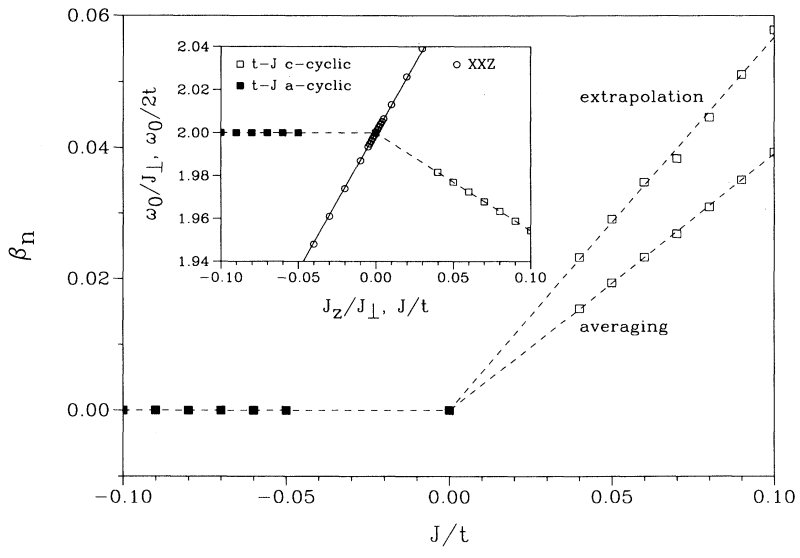

FIG. 8. The inset shows the dependence on the coupling constant of the renormalized bandwidth of the particle-hole spectrum, which is dynamically relevant for the dynamic structure factors $S_{zz}(q,\omega)$ of H_{XXZ} (circles) and $S_{nn}(q,\omega)$ of $H_{t\text{-}J}$ (squares) in the weak-coupling regimes. Each data point is derived from the continued-fraction coefficients $\Delta_2, \ldots, \Delta_5$ as explained in the text. The solid line represents the upper boundary $\varepsilon_U(\pi)$ of the spinon continuum. The dashed lines extrapolate the t-J data linearly into the region of very small coupling. The main plot shows the dependence on the coupling constant J/t of the infrared singularity exponent β_n in the charge dynamic structure factor $S_{nn}(\pi,\omega)$ of $H_{t\text{-}J}$, as inferred from the continued-fraction coefficients $\Delta_2, \ldots, \Delta_5$. The two sets of data for $J/t > 0$ result from two alternative methods as described in the text. The dashed lines extrapolate the data linearly into the region of very small coupling.

The results of that analysis are displayed in the main plot of Fig. 8. Again, only an antiferromagnetic exchange coupling ($J/t > 0$) affects the charge dynamics. Either method yields a smooth and approximately linear J/t dependence of β_n, which extrapolates convincingly toward the exact result $\beta_n = 0$ at $J/t = 0$. However, the two results differ significantly from each other. Unlike the sequences $\beta_z^{(k)}$ shown in the upper inset to Fig. 2, the corresponding $\beta_n^{(k)}$ sequences show no sign of convergence. We cannot expect, therefore, that extrapolation brings any improvement over averaging as was the case for β_z. It might instead be subject to significant systematic errors. We therefore conclude that our best result is

$$\beta_n \simeq 0.40 J/t, \tag{7.4}$$

obtained from averaging, more accurate in this case than the prediction $\beta_n \simeq 0.57 J/t$, inferred from extrapolation. Our result (7.4) for the infrared exponent β_n of the charge dynamic structure factor $S_{nn}(\pi,\omega)$ can be compared with the result of Ogata *et al.*[36] for the exponent K_ρ of the equal-time charge correlation function $\langle n_l n_{l+R}\rangle \sim (-1)^R R^{-4K_\rho}$. Under mild assumptions the relation between the two exponents is $4K_\rho = \beta_n + 2$. From a fit of the data points $K_\rho = 0.6$, 0.7 in Fig. 2 of Ref. 36 and the exact value $K_\rho = 0.5$ for J/t=0 (Refs. 2, 3, and 16) to a second-order polynomial we infer for the variation of K_ρ with J/t near the noninteracting limit the result $4K_\rho \simeq 2 + 0.41 J/t$, which is in near perfect agreement with (7.4).

E. Line shapes of $S_{nn}(\pi,\omega)$

The modified spectral-weight distributions in the charge dynamic structure factor $S_{nn}(\pi,\omega)$ of $H_{t\text{-}J}$ due to a weak positive exchange coupling J/t are qualitatively the same as those in the spin dynamic structure factor $S_{zz}(\pi,\omega)$ of H_{XXZ} due to a small negative $J_z/J_\perp$. The function $S_{zz}(\pi,\omega)$ has been described in Sec. IV, specifically in Fig. 4(b). The function $S_{nn}(\pi,\omega)$ at $J/t = 0.1$ as determined by the same method is shown in Fig. 9.

The many striking similarities of these two dynamic structure factors which have emerged from our weak-coupling continued-fraction analysis are, in fact, consistent with a study by Xiang and D'Ambrumenil[37] based on an approximate decoupling of the charge and spin degrees of freedom in $H_{t\text{-}J}$. In their approach, the charge dynamics remains governed by a Hamiltonian of spinless lattice fermions (as is rigorously the case at $J/t = 0$), and the weak exchange coupling is taken into account by an attractive fermion interaction. This model is very much akin to H_{XXZ} at $J_z/J_\perp < 0$ in the fermion representation. From that perspective it is not surprising that H_{XXZ} and $H_{t\text{-}J}$ exhibit very similar features in the corresponding dynamic structure factors: decreasing bandwidth, increasing infrared exponent, and the appearance of a discrete state near the band edge. Nevertheless, it is noteworthy that the effects of an antiferromagnetic spin coupling in $H_{t\text{-}J}$ are similar to what is in essence a ferromagnetic spin coupling in H_{XXZ}. All the observed features are much better understood in the context of H_{XXZ}. Their physical significance in the context of $H_{t\text{-}J}$ remains to be elucidated in full.

VIII. CONCLUSIONS

In this paper and in Ref. 1 we have presented the recursion method combined with techniques of continued-fraction analysis as a calculational tool for investigating the $T = 0$ dynamics of quantum many-body systems in both their weak-coupling and strong-coupling regimes. We have applied the method to one model (1D XXZ) for which some of our findings (spectral properties, infrared exponents) can be tested against exact results and to two models (2D XXZ and 1D t-J) for which no corresponding exact results exist. The main assets of this

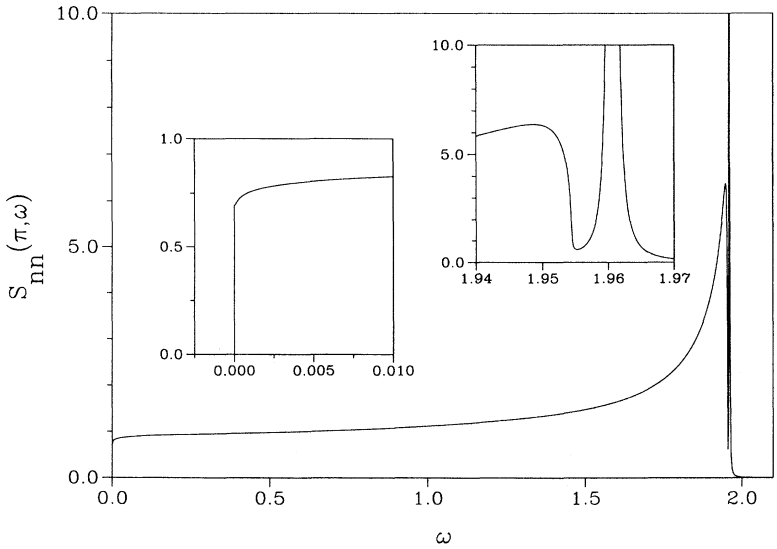

FIG. 9. Dynamic structure factor $S_{nn}(\pi,\omega)$ at $T = 0$ of the 1D t-J model (1.3) with $2t = 1$ and $J/t = 0.1$ obtained by a weak-coupling reconstruction from the nearly-size-independent continued-fraction coefficients $\Delta_1,\ldots,\Delta_5$. The method is the same as used for the XXZ results presented in Fig. 4. The insets show parts of the same function on expanded scales.

method are its general nature, its amenability to computational implementations, and the direct access it yields to dynamical quantities.

The method comprises two main tasks, which must be carried out with due circumspection in any given application: (i) In the calculation of continued-fraction coefficients for a specific dynamical variable from the ground-state wave function of a given Hamiltonian, special attention must be paid to finite-size effects, boundary conditions, special symmetries of small clusters, spurious level crossings, etc. (ii) The subsequent continued-fraction analysis in all its aspects (exponent analysis, gap analysis, reconstruction of spectral densities) then depends on whether the resulting Δ_k sequence indicates a weak-coupling regime or a strong-coupling regime.

In Ref. 1 we have introduced two model terminators that are suitable for strong-coupling applications under fairly general circumstances. They take into account the unbounded support of the pertinent spectral densities (with or without low-frequency gaps and infrared singularities). Weak-coupling applications such as described in this paper offer the advantage that the most suitable terminators can be constructed from the solution of the dynamical problem in the noninteracting limit. In this context it is important to note that the use of model-specific terminators does in no way limit or invalidate the generality of the method itself.

ACKNOWLEDGMENTS

This work was supported by the U.S. National Science Foundation, Grant No. DMR-93-12252. Computations were carried out on supercomputers at the National Center for Supercomputing Applications, University of Illinois at Urbana-Champaign. J.S. gratefully acknowledges the generous hospitality of the Department of Physics, University of Rhode Island, and the financial support of the Max Kade Foundation during the time when this work was begun.

---

* Present address: Department of Physics, North Dakota State University, Fargo, ND 58105-5566.

[1] V. S . Viswanath, S. Zhang, J. Stolze, and G. Müller, Phys. Rev. B **49**, 9702 (1994).

[2] E. Lieb, T. Schultz, and D. Mattis, Ann. Phys. (N.Y.) **16**, 407 (1961); S. Katsura, Phys. Rev. **162**, 1508 (1962).

[3] S. Katsura, T. Horiguchi, and M. Suzuki, Physica **46**, 67 (1970).

[4] T. Todani and K. Kawasaki, Prog. Theor. Phys. **50**, 1216 (1973).

[5] P. W. Anderson, Science **235**, 1196 (1987); F. C. Zhang and T. M. Rice, Phys. Rev. B **37**, 3759 (1988).

[6] C. Gros, R. Joynt, and T. M. Rice, Phys. Rev. B **36**, 381 (1987).

[7] The terms *c-cyclic* and *a-cyclic* were introduced by Lieb *et al.* (Ref. 2) for the lattice fermion representation of the XX model.

[8] B. M. McCoy, E. Barouch, and D. B. Abraham, Phys. Rev. A **4**, 2331 (1971).

[9] R. Haydock, Solid State Phys. **35**, 215 (1980).

[10] *The Recursion Method and its Applications*, edited by D. G. Pettifor and D. L. Weaire (Springer-Verlag, New York, 1985).

[11] M. H. Lee, Phys. Rev. B **26**, 2547 (1982).

[12] E. R. Gagliano, E. Dagotto, A. Moreo, and F. C. Alcaraz, Phys. Rev. B **34**, 1677 (1986).

[13] V. S. Viswanath and G. Müller, J. Appl. Phys. **67**, 5486 (1990); **70**, 6178 (1991).

[14] V. S. Viswanath and G. Müller, *Recursion Method—Application to Many-Body Dynamics*, Lecture Notes in Physics Vol. m 23 (Springer-Verlag, New York, 1994).

[15] A. Luther and I. Peschel, Phys. Rev. B **12**, 3908 (1975).

[16] T. Niemeijer, Physica **36**, 377 (1967).

[17] J. Des Cloizeaux and M. Gaudin, J. Math. Phys. **7**, 1384 (1966).

[18] A. Magnus, Ref. 10, p. 22.

[19] In the fermion representation, the operator $A = S_q^x$ couples to excitations involving arbitrarily many fermions even in the noninteracting limit.

[20] In the reconstructed relaxation function $\tilde{c}_0(z)$ the discrete state is represented by an isolated pole. For $z = \epsilon - i\omega$ with $\epsilon = 0.0001$, it has a small but visibly nonzero width.

[21] J. D. Johnson, S. Krinsky, and B. M. McCoy, Phys. Rev. A **6**, 1613 (1973).

[22] G. Müller and R. E. Shrock, Phys. Rev. B **29**, 288 (1984).

[23] A numerically stable algorithm which transforms frequency moments into continued-fraction coefficients and vice versa can be found in Ref. 1.

[24] A plot of the first 15 Δ_k's of (5.1) can be found in Ref. 13, where they were used to test some aspects of the continued-fraction analysis used here.

[25] As a test we have reconstructed the exact result (5.1) with the coefficients $\Delta_1, \ldots, \Delta_5$ from the finite system and found a result that agrees with dashed curve in Fig. 5 to within line thickness. The only visible deviation was a slight rounding of the cusp at $\omega' = 1$.

[26] In Ref. 13 we have been able to estimate the exponent $\beta_z + 1$ for the case $J_z/J_\perp = 0$ on the basis of 15 Δ_k's.

[27] T. Schneider, E. Stoll, and U. Glaus, Phys. Rev. B **26**, 1321 (1982).

[28] H. Beck and G. Müller, Solid State Commun. **43**, 399 (1982).

[29] It was pointed out in Ref. 27 that for $J_z/J_\perp > 0$ the Hartree-Fock analysis predicts a spurious branch of bound states below the spinon continuum. No such artifact occurs in the weak-coupling continued-fraction analysis.

[30] H. C. Fogedby, J. Phys. C **11**, 4767 (1978).

[31] G. Müller, H. Thomas, H. Beck, and J. C. Bonner, Phys. Rev. B **24**, 1429 (1981); G. Müller, H. Thomas, M. W. Puga, and H. Beck, J. Phys. C **14**, 3399 (1981).

[32] S. E. Nagler, D. A. Tennant, R. A. Cowley, T. G. Perring, and S. K. Satija, Phys. Rev. B **44**, 12361 (1991); D. A. Tennant, T. G. Perring, R. A. Cowley, and S. E. Nagler, Phys. Rev. Lett. **70**, 4003 (1993).

[33] The hopping term of $H_{t\text{-}J}$ leaves the sequence of spin orientations invariant.

[34] The additional symmetries of the four-site lattice give rise to further degeneracies, which are unimportant for our discussion.

[35] The near degeneracy of the t-J ground state at very small $|J/t|$ poses a computational problem for the recursion method, specifically for the numerical determination of the ground-state wave function via a recursive algorithm (e.g., modified Lanczos or conjugate gradient).

[36] M. Ogata, M. U. Luchini, S. Sorella, and F. F. Assaad, Phys. Rev. Lett. **66**, 2388 (1991).

[37] T. Xiang and N. D'Ambrumenil, Phys. Rev. B **45**, 8150 (1992).